

## AN APPLICATION OF THE FINITE VOLUME METHOD TO THE BIO-HEAT-TRANSFER-EQUATION IN PREMATURE INFANTS \*

MARTIN LUDWIG<sup>†</sup>, JOCHIM KOCH<sup>‡</sup>, AND BERND FISCHER<sup>†</sup>

*In memory of Gene Golub*

**Abstract.** In this report the development of a finite volume method for the time-accurate simulation of the temperature distribution in a premature infant inside an incubator or in an open radiant warmer is described. The real geometry of a premature infant is obtained from MRT-images. The infants thermoregulation is modelled by the so-called bio-heat-transfer-equation incorporating source terms and Neumann boundary conditions. The source terms describe the metabolic heat production, the blood flow and the respiratorical water loss whereas the Neumann boundary conditions model the heat transfer by transepidermal water loss, radiation, convection and conduction. The numerical solution is carried out by the developed finite volume method whose spatial discretization is done by a 3D-mesh-generator from CFD. For the time integration a semi-implicit multistep method is used. The arising large, sparse linear systems are efficiently solved with a Krylov subspace method. Some successful test runs using real life data are presented.

**Key words.** premature infant, bio-heat-transfer-equation, finite volume method, BiCGStab

**AMS subject classifications.** 65M, 92C

**1. Introduction.** In Germany 7% of all newborn babies are preterm, corresponding to about 55,000 of about 800,000 newborn babies per year. Reasons for a premature birth may be diseases of the mother (e.g. high blood pressure, diabetes) or sudden complications like infections or shocks. But nevertheless for about half of all premature births no reason can be found. In order to protect premature infants against heat- and water-losses to their surroundings, against infections and hypoxemia, incubators and open radiant warmers are widely used. A description of how these devices work and their history of development can be found in [11], an introduction to the general principles of thermoregulation of premature infants in [7].

To better understand the thermoregulation of premature infants in a certain micro-climate, thermoregulatory models and corresponding simulation tools have been developed. Using them it is possible to gain insight into the involved processes and the complexity of the whole thermoregulatory system. They are systematic tools for hyperthermia planning and for the improvement of warming therapy devices. They allow for clinical studies and for the prediction of physiological phenomena without exposing human beings to experiments. In a clinical setting, a sound simulation of the thermoregulation would allow for a proper tuning of the environmental parameter within the incubator with the goal to achieve the optimal living conditions for the specific newborn.

Hardware simulators (manikins, dummies) are an approach to model the thermoregulatory system. Because it is difficult to manufacture them and nearly impossible to adjust them to new parameters, quantitative models have been of keen interest to scientists and engineers for a long time. The work of Bußmann [4] is a milestone of physiological developments. It contains a synopsis of the physiological basics of thermoregulation and the development of a computer model to simulate the dynamic heat transfer processes of a preterm or newborn baby in an incubator. The processes of molecular heat transfer, metabolic heat production

---

\*Received October 9, 2006. Accepted for publication March 15, 2007. Recommended by A. Wathen. This work was supported by the Technology Foundation of Schleswig-Holstein.

<sup>†</sup>University of Lübeck, Institute of Mathematics, Wallstraße 40, 23560 Lübeck, Germany (fischer@math.uni-luebeck.de).

<sup>‡</sup>Drägerwerk AG, Dept. of Basic Development, Moislinger Allee 53-55, 23542 Lübeck, Germany.

and heat transfer due to blood flow are modelled as well as the heat losses over the skin by transepidermal water loss, radiation, and convection. Furthermore the control mechanisms thermogenesis without shivering and vasomotoric control of the skin are taken into account. Nevertheless the disadvantages of the model are obvious. The geometry of an infant is replaced by a non-realistic compartment model and only homogeneous temperature profiles can be computed.

The series of works by Fischer et al. [10], Fenner [8] and Wronna [20] has taken first steps towards a more realistic modeling. The work [16] presents the development of a numerical method for the time-accurate computation of the temperature distribution inside a premature infant. It is an essential improvement of the model presented in [4], because it allows for simulations in realistic 3-dimensional geometries. Furthermore the dynamic evolution of the temperature distributions can be computed. In addition not only incubator settings, but also the conditions of an open radiant warmer are modelled. Besides, the boundary conditions are modified and a new one for conduction is introduced.

The present paper is a brief summary of [16]. Section 2 describes the modeling and computer simulation of the real geometry of a premature infant by means of MRT-slices and the use of a CFD-grid-generator. In section 3 the mathematical model is outlined. It is an initial boundary value problem (IBVP) consisting of the bio-heat-transfer-equation (BHTE) supplemented by initial and boundary Neumann conditions. The BHTE describes the temperature distribution inside the preterm baby taking into account the molecular heat transfer, metabolic heat production, heat transfer due to blood flow and respiratorical water loss. In order to solve the BHTE numerically, section 4 surveys the constituent parts of a finite volume method. First, finite volume methods are a natural choice for the numerical solution of the BHTE because they are directly applicable to its integral form. Second, the use of unstructured grids is necessary in order to cope with realistic geometries. Finite volume methods are formulated on general control volumes and hence can easily be employed on unstructured grids, indeed one can even say that they are especially designed for such grids. In section 5 numerical test runs using real life data are presented.

**2. Modeling the real geometry of a premature infant.** Figure 2.1 is an MRT-image showing a sagittal intersection of a premature infants body. Using a bulk of such MRT-images in a commercial image processing tool, which supplies segmentation-tools, especially the Region Growing, a volume image is generated; see Figure 2.2. The subsequent application of the so-called marching cube algorithm (see [15]) to this volume image yields the baby's surface and in addition to that a surface triangulation; see Figure 2.3. The implementation of a finite volume method on a computer requires the decomposition of the computational domain into sub-domains of a simple shape, so-called control volumes. A control volume  $\sigma_i$  is a subset on which the Gaussian divergence-theorem holds, for example a cube or a prism. Using the obtained surface triangulation as input data, a grid generator from CFD yields a 3D-mesh  $D \subset \mathbb{R}^3$  as a model of the infant's body; see Figure 2.4. Here, the interior points were selected according to the known layer size of the considered compartments, starting from the skin, i.e., from the computed surface triangulation. The computational mesh includes 5,262 surface-triangles and 101,930 control-volumes.

**3. Governing equations.** This section contains the essence of a thermoregulatory model described in detail by Ludwig [16]. The baby lies on a mattress in an incubator or in an open radiant warmer. Its body model  $D \subset \mathbb{R}^3$  consists of the compartments head, trunk and periphery (arms and legs). The head is composed of the 4 layers skin, fat, bone and kernel (brain), the trunk and the periphery only of the 3 layers skin, fat and kernel. The regular boundary of the body model is denoted by  $\partial_r D \subset \partial D$ . Here  $n : \partial_r D \rightarrow \mathbb{R}^3$  is the outer unit-normal-vector-field upon this regular boundary. The infants are classified by the basic

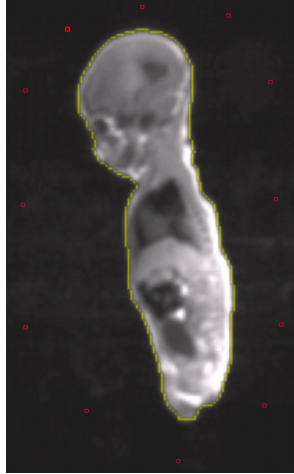


FIG. 2.1. MRT-slice



FIG. 2.2. Volume image

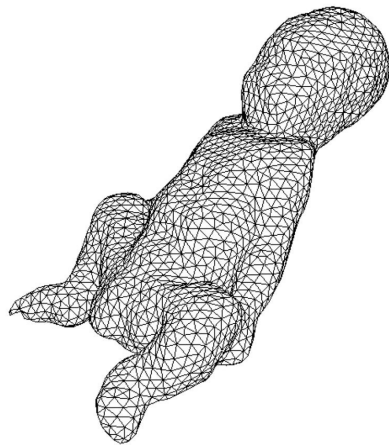


FIG. 2.3. Surface triangulation

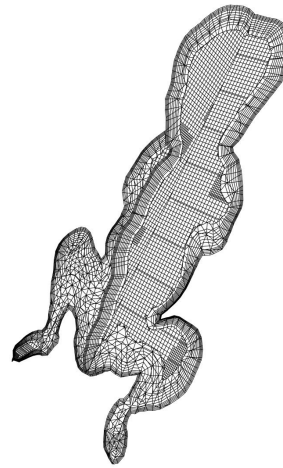


FIG. 2.4. Sagittal and coronal intersection of the 3D-mesh

parameters gestational age, post-natal age and weight. Moreover,  $T(x, t) > 0$  denotes the temperature in Kelvin with space variable  $x \in \mathbb{R}^3$  and time  $t \geq 0$  ( $[x] = m^3$ ,  $[t] = sec.$ ). The 3 functions  $\lambda$ ,  $c$  and  $\rho$  describe the heat conductivity, specific heat and density of the involved tissues. According to Fourier's fundamental law of molecular heat transfer the heat flux is given by

$$J : \bar{D} \times \mathbb{R}_+^* \rightarrow \mathbb{R}^3, \quad J(x, t) := -\lambda(x) \cdot \nabla T(x, t).$$

The divergence of the the field  $-J$  then describes the molecular heat transfer. The differential operators  $\nabla$  and  $div$  always refer to differentiation in space only. The production terms

$$Q^{Met}(T, x, t), \quad Q^{Blood}(T, x, t), \quad Q^{RW}(x),$$

model the metabolic heat production, the heat transfer due to blood flow and the heat loss due to respiratorical water loss. Because a detailed derivation would be far beyond the scope of this report, the reader is referred to [16]. The terms

$$M^{TW}(T, x, t), \quad M^r(T, x, t), \quad M^{cv}(T, x, t), \quad M^{cd}(T, x, t),$$

model the heat fluxes over the skin by transepidermal water loss, radiation, convection and conduction, respectively. Setting  $\kappa(x) := \rho(x)c(x)$ , the temperature distribution  $T : \mathbb{R}^3 \times \mathbb{R}_+ \rightarrow \mathbb{R}$  satisfies the bio-heat-transfer-equation

$$(3.1) \quad \begin{aligned} \kappa(x) \frac{\partial T}{\partial t}(x, t) &= \operatorname{div}(-J)(x, t) + \mathcal{Q}^{Met}(x, t) + \mathcal{Q}^{Blut}(x, t) + \mathcal{Q}^{RW}(x), \\ (x, t) &\in D \times \mathbb{R}_+^* \end{aligned}$$

(see [17, 1]), which is supplemented by the initial and boundary conditions

$$(3.2) \quad T(x, 0) = T_0(x), \quad x \in D,$$

$$(3.3) \quad \begin{aligned} \langle J(x, t), n(x) \rangle &= M^{TW}(x, t) + M^r(x, t) + M^{cv}(x, t) + M^{cd}(x, t), \\ (x, t) &\in \partial_r D \times \mathbb{R}_+^*. \end{aligned}$$

Here  $T_0 : D \rightarrow \mathbb{R}$  is an initial temperature distribution in  $D$ . Exact solutions of (3.1) can only be found in very few cases. Therefore a numerical treatment is often necessary.

**4. Finite volume approximation.** Since finite volume methods are especially designed for equations incorporating divergence terms, they are a good choice for the numerical treatment of the bio-heat-transfer-equation (3.1). Their basic idea is to eliminate the divergence-terms by applying the Gaussian divergence theorem. As a result the order of derivatives is reduced by one. Furthermore they allow for complex geometries and unstructured grids, which is another reason to use them for (3.1).

In this section the development of a finite volume method for (3.1), (3.2) and (3.3) is concisely presented. It consists of a spatial and a time discretization. The former requires a suitable transformation of the given initial boundary value problem. Subsequently an evolution equation for mean temperatures on the control-volumes  $\sigma_i$  is derived. The application of the method of lines (MOL) then yields a high-dimensional system of ordinary differential equations (ODE-system). The subsequent time integration is done by the SBDF(3)-method, which belongs to the class of semi-implicit multistep methods (IMEX-methods). The arising large, sparse linear systems are efficiently solved by the BiCGStab method with an ILU preconditioning.

For an introductory analysis of the finite volume technique the reader is referred to [9].

#### 4.1. Spatial discretization. Setting

$$\mathcal{Q}(x, t) := \mathcal{Q}^{Met}(x, t) + \mathcal{Q}^{Blood}(x, t) + \mathcal{Q}^{RW}(x), \quad (x, t) \in D \times \mathbb{R}_+^*,$$

$$\varphi(x, t) := M^{TW}(x, t) + M^r(x, t) + M^{cv}(x, t) + M^{cd}(x, t), \quad (x, t) \in \partial_r D \times \mathbb{R}_+^*,$$

the given IBVP reads

$$\kappa(x) \frac{\partial T}{\partial t}(x, t) = \operatorname{div}(-J)(x, t) + \mathcal{Q}(x, t), \quad (x, t) \in D \times \mathbb{R}_+^*,$$

$$T(x, 0) = T_0(x), \quad x \in D,$$

$$\langle J(x, t), n(x) \rangle = \varphi(x, t), \quad (x, t) \in \partial_r D \times \mathbb{R}_+^*.$$

In order to apply the finite volume technique, the IBVP has to be transformed into pure divergence form. This means that the time derivative as well as the divergence term must not be multiplied by any function of the space variable  $x$ . Consequently, division by  $\kappa(x)$  is not allowed. Defining the transformed temperature

$$u : \mathbb{R}^3 \times \mathbb{R}_+ \rightarrow \mathbb{R}, \quad u(x, t) := \kappa(x)T(x, t),$$

and the transformed heat flux field

$$v : \mathbb{R}^3 \times \mathbb{R}_+^* \rightarrow \mathbb{R}^3, \quad v(x, t) := \frac{\lambda(x)}{\kappa(x)} \nabla u(x, t) - \frac{\lambda(x)u(x, t)}{\kappa^2(x)} \nabla \kappa(x),$$

the BHTE is equivalent to

$$(4.1) \quad \frac{\partial u}{\partial t}(x, t) = \operatorname{div} v(x, t) + \mathcal{Q}(x, t), \quad (x, t) \in D \times \mathbb{R}_+^*$$

(see [3], [20]). Setting  $u_0(x) := \kappa(x)T_0(x)$ ,  $x \in D$ , the transformation of the initial condition yields

$$(4.2) \quad u(x, 0) = u_0(x), \quad x \in D,$$

whereas the transformed Neumann boundary condition reads

$$(4.3) \quad \langle v(x, t), n(x) \rangle = -\varphi(x, t), \quad (x, t) \in \partial_r D \times \mathbb{R}_+^*.$$

Equations (4.1), (4.2) and (4.3) constitute an IBVP for the transformed temperature  $u$ .

**DEFINITION 4.1.** *Given a non-empty control volume  $\sigma_i \subset D$ , the (spatial) cell average of  $u$  is defined by*

$$u_i(t) := \frac{1}{|\sigma_i|} \int_{\sigma_i} u(x, t) dx, \quad t \in \mathbb{R}_+^*,$$

where  $|\sigma_i|$  denotes the volume of  $\sigma_i$ .

Let  $\sigma_i \subset D$  be a non-empty control volume. The evolution in time of the associated cell average is described by

$$\frac{du_i}{dt}(t) = \frac{1}{|\sigma_i|} \int_{\sigma_i} \frac{\partial u}{\partial t}(x, t) dx = \frac{1}{|\sigma_i|} \left( \int_{\sigma_i} \operatorname{div} v(x, t) dx + \int_{\sigma_i} \mathcal{Q}(x, t) dx \right), \quad t \in \mathbb{R}_+^*.$$

Using the Gaussian divergence theorem yields the evolutionary equation

$$(4.4) \quad \frac{du_i}{dt}(t) = \frac{1}{|\sigma_i|} \left( \int_{\partial\sigma_i} \langle v(x, t), n^i(x) \rangle dS(x) + \int_{\sigma_i} \mathcal{Q}(x, t) dx \right), \quad t \in \mathbb{R}_+^*.$$

Here  $n^i : \partial_r \sigma_i \rightarrow \mathbb{R}^3$  denotes the outer unit-normal-vector-field upon the regular boundary of the cell  $\sigma_i$ . A finite volume method is a discretization of all evolutionary equations given by (4.4).

Given two control volumes  $\sigma_i \subset D$  and  $\sigma_j \subset D$ , their common boundary in the interior of  $D$  is denoted by  $f_{ij}$ . Given a control-volume  $\sigma_i \subset D$  situated at the boundary of  $D$ , a triangle of the surface triangulation being part of the boundary  $\partial\sigma_i$  is denoted by  $\bar{f}_{ij}$ . For a control volume  $\sigma_i$ ,  $N(i)$  is defined as the number of boundary parts in the interior of  $D$ .

Accordingly,  $\overline{N}(i)$  is defined as the number of boundary parts on the surface of the body, which therefore are triangles. The functions

$$\begin{aligned}\mathcal{L}_i^{IFL}(t) &:= \sum_{j=1}^{N(i)} \int_{f_{ij}} \langle v(x, t), n^i(x) \rangle dS(x), \quad t \in \mathbb{R}_+^*, \quad i \in \{1, \dots, N\}, \\ \mathcal{L}_i^{RFL}(t) &:= \sum_{j=1}^{\overline{N}(i)} \int_{\bar{f}_{ij}} \langle v(x, t), n^i(x) \rangle dS(x), \quad t \in \mathbb{R}_+^*, \quad i \in \{1, \dots, N\}, \\ \mathcal{L}_i^Q(t) &:= \int_{\sigma_i} \mathcal{Q}(x, t) dx, \quad t \in \mathbb{R}_+^*, \quad i \in \{1, \dots, N\},\end{aligned}$$

describe the heat fluxes over the interior boundary parts and the surface triangles, and the energy production by the source terms, respectively, where  $N$  is the total number of control volumes. Now the evolutionary equation of the cell averages takes the form

$$(4.5) \quad \frac{du_i}{dt}(t) = \frac{1}{|\sigma_i|} \left( \mathcal{L}_i^{IFL}(t) + \mathcal{L}_i^{RFL}(t) + \mathcal{L}_i^Q(t) \right), \quad t \in \mathbb{R}_+^*, \quad i \in \{1, \dots, N\}.$$

The modelled processes molecular heat transfer, boundary conditions (transepidermal water loss, radiation, convection, conduction) and source terms (metabolic heat production, heat transfer due to blood flow, heat loss due to respiratorical water loss) are reflected very clearly by this equation. They determine the evolution in time of the cell average. Equation (4.5) constitutes an ODE system whose dimension is the total number of control volumes.

Next, the functions  $\mathcal{L}_i^{IFL}$ ,  $\mathcal{L}_i^{RFL}$  and  $\mathcal{L}_i^Q$  have to be approximated by quadrature formulas. Since this is far beyond the scope of this text, it is omitted here and the reader is referred to [16] again. We determine approximating functions  $L_i^{IFL}$ ,  $L_i^{RFL}$  and  $L_i^Q$ , and the discretized evolutionary equation reads

$$(4.6) \quad \frac{du_i}{dt}(t) \approx \frac{1}{|\sigma_i|} \left( L_i^{IFL}(t) + L_i^{RFL}(t) + L_i^Q(t) \right), \quad t \in \mathbb{R}_+^*, \quad i \in \{1, \dots, N\}.$$

**4.2. Time discretization.** The approximating functions in (4.6) can be separated in affine-linear and non-linear parts (see [16]). Let

$$u(t) := \begin{pmatrix} u_1(t) \\ \vdots \\ u_N(t) \end{pmatrix} \in \mathbb{R}^N, \quad t \in \mathbb{R}_+^*,$$

be a vector containing all cell averages. With a vector  $D^i \in \mathbb{R}^N$ , a real number  $d_i$  and a function  $L_i$  describing the non-linear parts, one can write

$$(4.7) \quad \frac{du_i}{dt}(t) \approx \frac{1}{|\sigma_i|} \left( D^{iT} u(t) + d_i + L_i(t) \right), \quad t \in \mathbb{R}_+^*, \quad i \in \{1, \dots, N\}.$$

Since the term  $D^{iT} u(t) + d_i$  originates from diffusion processes, the system (4.7) is likely to be stiff. Since the time integration of such systems is very difficult, stable schemes have to be applied; see [5, 12]. The implicit BDF schemes are the best choice, because they allow for relatively large time steps. Consequently, moderate computation times can be expected. However, in each time step a system of equations has to be solved. In this work the implicit BDF(3) scheme is used as a basic scheme for time-integration. Yet a fully implicit treatment

of the function  $L_i$  would result in memory requirements which cannot be satisfied in general; cf. [16]. Therefore, an extrapolation procedure is applied to  $L_i$ , which leads to the SBDF(3) scheme (semi-implicit BDF scheme; see [2]). With the discretized time base

$$0 = t_0 < t_1 < t_2 < \dots, \quad t_n := n\Delta t, \quad n \in \mathbb{N}, \quad \Delta t \in \mathbb{R}_+^*,$$

the approximating cell average vectors

$$u^0 = \begin{pmatrix} u_1^0 \\ \vdots \\ u_N^0 \end{pmatrix} := \begin{pmatrix} u_0(x^1) \\ \vdots \\ u_0(x^N) \end{pmatrix}, \quad u^n = \begin{pmatrix} u_1^n \\ \vdots \\ u_N^n \end{pmatrix} \approx \begin{pmatrix} u_1(t_n) \\ \vdots \\ u_N(t_n) \end{pmatrix} = u(t_n), \quad n \in \mathbb{N}^*,$$

and the update vector

$$\Delta u^n = \begin{pmatrix} \Delta u_1^n \\ \vdots \\ \Delta u_N^n \end{pmatrix} := \begin{pmatrix} u_1^{n+1} - u_1^n \\ \vdots \\ u_N^{n+1} - u_N^n \end{pmatrix} = u^{n+1} - u^n, \quad n \in \mathbb{N},$$

the SBDF(3) scheme applied to (4.7) reads for  $n \geq 0$  and  $i \in \{1, \dots, N\}$ ,

$$\begin{aligned} & \frac{11}{6}u_i^{n+3} - 3u_i^{n+2} + \frac{3}{2}u_i^{n+1} - \frac{1}{3}u_i^n \\ &= \Delta t \left[ \frac{1}{|\sigma_i|} \left( D^{iT} u^{n+3} + d_i \right) + \frac{3}{|\sigma_i|} L_i^{n+2} - \frac{3}{|\sigma_i|} L_i^{n+1} + \frac{1}{|\sigma_i|} L_i^n \right]. \end{aligned}$$

Setting

$$r_i^n := \frac{\Delta t}{|\sigma_i|} \left[ d_i + 3L_i^{n+2} - 3L_i^{n+1} + L_i^n \right] \in \mathbb{R}, \quad n \geq 0, \quad i \in \{1, \dots, N\},$$

a straightforward calculation with  $n \geq 0$ ,  $i \in \{1, \dots, N\}$  shows that

$$(4.8) \quad \begin{aligned} & \left( \frac{11}{6}e^i - \frac{\Delta t}{|\sigma_i|} D^i \right)^T \Delta u^{n+2} \\ &= \left( \frac{7}{6}e^i + \frac{\Delta t}{|\sigma_i|} D^i \right)^T u^{n+2} - \frac{3}{2}e^{iT} u^{n+1} + \frac{1}{3}e^{iT} u^n + r_i^n. \end{aligned}$$

Equation (4.8) yields a sparse linear system of dimension  $N \times N$ . It is solved for the update  $\Delta u^{n+2}$ ,  $n \geq 0$ , in the  $(n+3)$ rd time step. Starting values are computed with a semi-implicit one-step method.

We remark that in order to achieve an appropriate resolution of the computational domain  $D$ , the total number of cells is chosen very large ( $N = 101930$ , cf. section 2). Therefore the linear systems (4.8) obtained are too large to be solved by a direct method. Among the most well-known iterative solvers being applicable to a non-symmetric system are the Krylov subspace methods. Here, we applied successfully the BiCGStab method developed by van der Vorst [19]. For preconditioning an incomplete LU factorization (ILU) is applied. It is worthwhile noting that the matrix of the system (4.8) is constant. Thus its entries have to be calculated only once at the beginning of the whole computation. The same holds for the ILU preconditioning.



TABLE 5.1  
*Material properties in  $[\frac{W}{mK}]$ ,  $[\frac{J}{kgK}]$ ,  $[\frac{kg}{m^3}]$ .*

	$\lambda$	$c$	$\rho$
skin	0.35	3770.0	1030.0
fat	0.21	2500.0	1030.0
bone	0.40	2170.0	1030.0
kernel	0.51	3770.0	1030.0

TABLE 5.2  
*Boundary condition sets.*

	$T_{air}$	$rH$	$T_{sur}$	$T_{MRT}$	$S_{MRT}$	$FL$	$k_{mat}$	$T_{mat}$
RBD1	309.25 K	77.0	293.15 K	297.6 K	$0.0 \frac{W}{m^2}$	$5.0 \frac{cm}{s}$	$0.05 \frac{W}{m^2K}$	309.25 K
RBD2	293.15 K	50.0	293.15 K	293.15 K	$140.0 \frac{W}{m^2}$	$30.0 \frac{cm}{s}$	$14.0 \frac{W}{m^2K}$	312.15 K

**5. Numerical results.** This section presents the results of numerical tests. They were carried out by the developed finite volume method for an infant whose weight, gestational age, and post-natal age was 1,240 kg, 32 weeks, and 3 days, respectively. The layer thicknesses of the involved tissues were estimated by statistical means; cf. [4]. Their values are 0.001 m for skin and fat and 0.005 m for bone. The heat conductivities, specific heats and specific weights of the involved tissues are listed in Table 5.1; see [6, 18]. Note that skin, fat, bone, and kernel are from a clinical point of view the relevant parts to be considered.

The boundary condition sets listed in Table 5.2 were used for the numerical test runs. The set values determine the heat fluxes over the infant's skin (cf. section 3). The set RBD1 describes the standard case, i.e., the incubator stands in a room with a given temperature  $T_{surround}$  and the air velocity  $FL$  inside the incubator is pre-set. The infant lies on an insulating mattress with known heat-transfer-coefficient  $k_{mat}$ . The air temperature  $T_{air}$  and the relative humidity  $rH$  of the incubator have been calculated with the optimization tool [13]. The temperature of the mattress is chosen equal to the air temperature,  $T_{mat} = T_{air}$ . The radiation temperature  $T_{MRT}$  of the incubator is given by its interior wall temperature.  $S_{MRT}$  denotes the power supply of a radiant heater and is set to zero, cause no radiant heater is taken into account in the incubator case.

The boundary condition set RBD2 describes the case of the open radiant warmer. It stands in a room with a given temperature  $T_{surround} = T_{air}$  and the air velocity  $FL$  inside this room is known. The room is air conditioned with a relative humidity of 50%. The radiation temperature  $T_{MRT}$  is given by the wall temperature which is identical with the air temperature, i.e.  $T_{MRT} = T_{air} = T_{surround}$ . The radiative power supply  $S_{MRT}$  was estimated with the simulation tool [14]. The infant lies upon a heated mattress with known heat transfer coefficient  $k_{mat}$  and temperature  $T_{mat}$ .

Three representative of altogether six numerical test runs are presented here. Their main features are listed in Table 5.3. The test cases TEST1a and TEST1b refer to the incubator case, whereas TEST2 describes the infant in the open radiant warmer. The only difference between TEST1a and TEST1b is the activity of the source terms. In order to better demonstrate their effects, TEST1a is treated with heat production and without blood flow, whereas TEST1b is treated with both of them.

*Remarks concerning the test runs:*

1. TEST1a starts with a constant initial temperature distribution of  $T_0(x) = 310.15K = 37^\circ C$  (cf. (3.2)). TEST1b starts with the temperature distribution of TEST1a after 60 minutes. TEST2 starts with the temperature distribution of a test case not presented here.



TABLE 5.3  
Test cases.

	B. c. set	$t_0$	$t_E$	$\Delta t$	$n_{max}$	Heat- prod.	Blood- flow	Resp. water losses
TEST1a	RBD1	0.0 s	3600 s	0.1 s	36000	on	off	off
TEST1b	RBD1	0.0 s	3600 s	0.1 s	36000	on	on	off
TEST2	RBD2	0.0 s	2700 s	0.1 s	27000	on	on	on

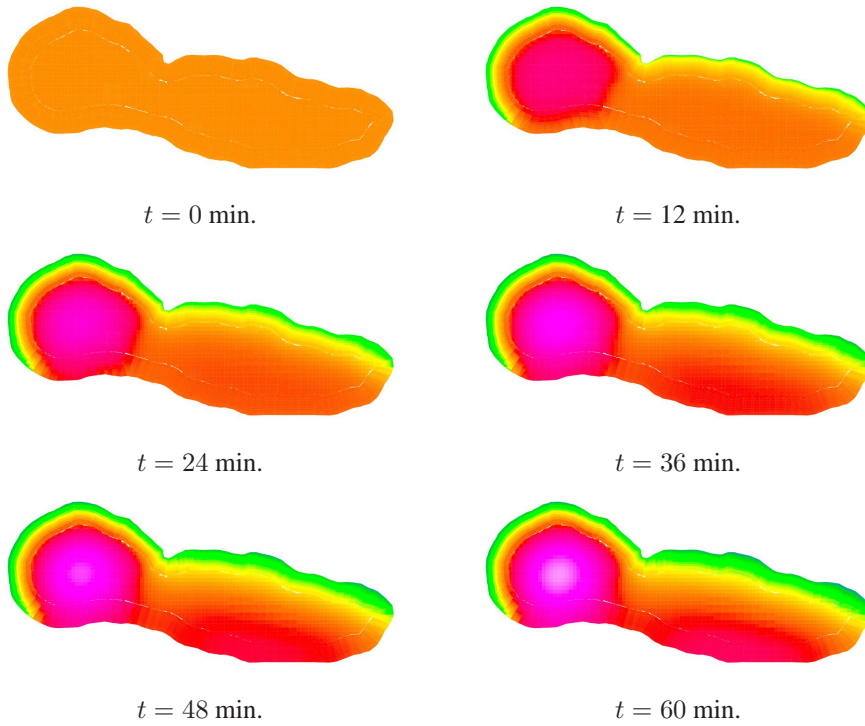


FIG. 5.1. TEST1a.

2. For each test run the maximum time step size for a stable integration was determined by numerical experiments. Thereafter, we tried even finer steps. The obtained heat distributions were visually indistinguishable from the displayed ones. For the retransformed temperature vectors

$$T^n := \left( \frac{u_1^n}{\kappa(x^1)}, \dots, \frac{u_N^n}{\kappa(x^N)} \right)^T \in \mathbb{R}^N, \quad n \geq 0,$$

the update vectors

$$\Delta T^n := T^{n+1} - T^n = \left( \frac{\Delta u_1^n}{\kappa(x^1)}, \dots, \frac{\Delta u_N^n}{\kappa(x^N)} \right)^T \in \mathbb{R}^N, \quad n \geq 0,$$

were computed. A typical convergence plot is depicted in Figure 5.5. The convergence criterion  $\|\Delta T^n\|_\infty < 5 \cdot 10^{-5} K$  was chosen and  $t_E$  denotes the corresponding stopping time. The total number of time steps is given by  $n_{max} = \frac{t_E - t_0}{\Delta t} = \frac{t_E}{\Delta t}$ .

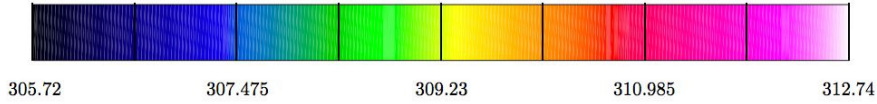


FIG. 5.2. Scale of temperature in [K].

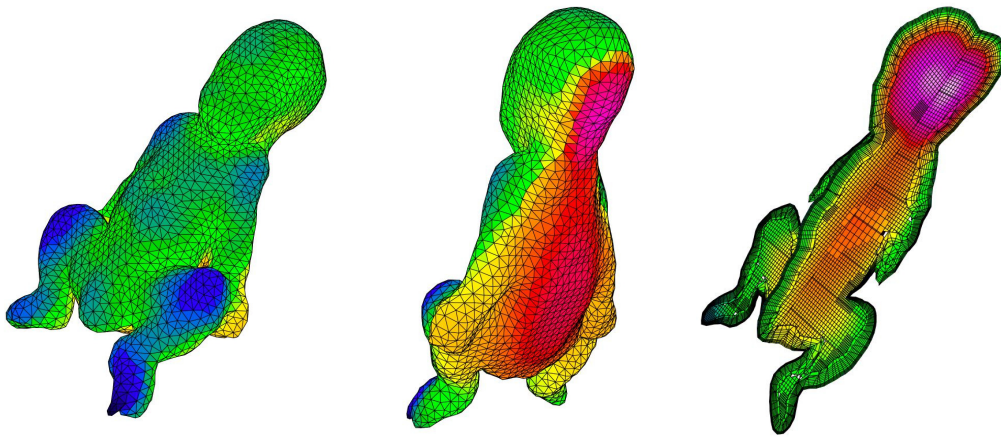


FIG. 5.3. TEST1a at  $t = 60$  min.

3. The stopping criterion for the residual of the incorporated linear solver BiCGStab with ILU preconditioning was set to  $\varepsilon = 10^{-10}$ .

4. All test runs were carried through on an AMD Athlon XP2700+ with 1 GB RAM. Table 5.4 contains computing times and the number of required time steps to satisfy the convergence criterion.

TABLE 5.4  
Computing times and time steps.

	Computing time	Time steps
TEST1a	2 h 28 min	$3.5 \times 10^4$
TEST1b	2 h 31 min	$3.6 \times 10^4$
TEST2	1h 54 min	$2.7 \times 10^4$

*Remarks concerning the temperature distributions:* Figures 5.1, 5.3, 5.4, 5.6, and 5.7 visualize the obtained temperature distributions. The time evolution in a sagittal intersection as well as the temperature distributions on the surface are shown

1. TEST1a (Figures 5.1 and 5.3) is a test case for the heat production. Corresponding to the distribution of heat production inside the body, the global temperature maximum is settled in the brain region whereas a local temperature maximum is built up in the kernel of the trunk. These two concentrations of heat energy are superimposed by the cooling effect of the air and by the insulating effect of the mattress. These effects also can be observed in the surface temperature distributions in Figure 5.3: The lowest temperatures occur on the top side of the infant. This is due to the cooling effect of the air as well as to the low heat production in the periphery. The highest temperatures occur at the back side of the infant. Again the global temperature maximum in the brain is prominent.

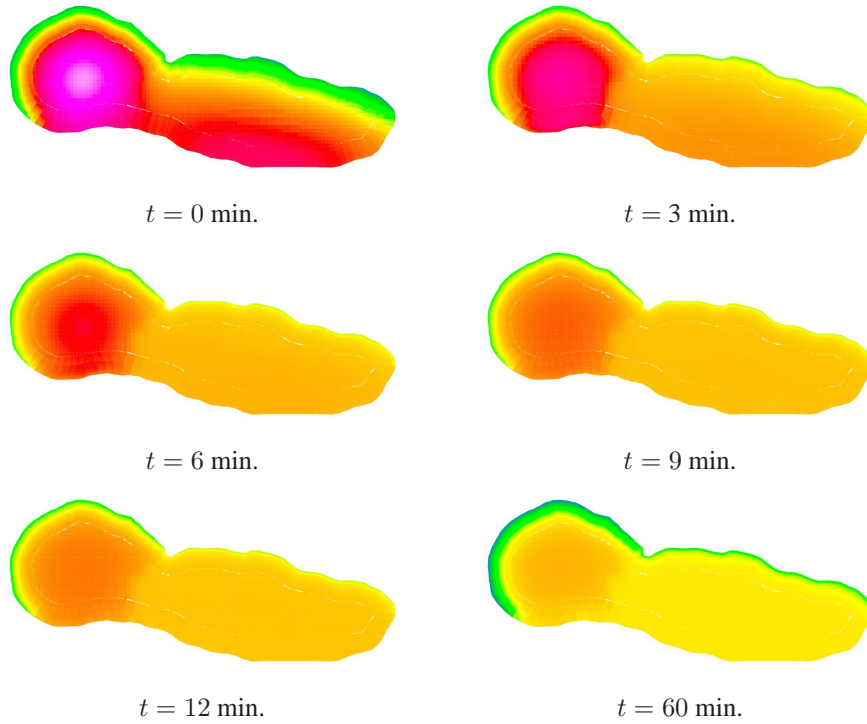


FIG. 5.4. *TEST1b*.

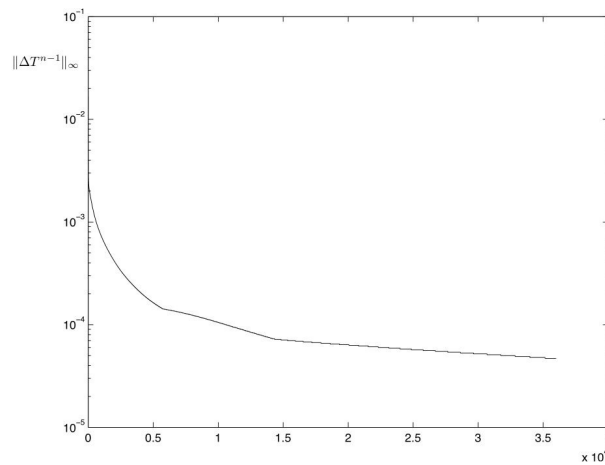


FIG. 5.5. *Convergence history: Number of time steps vs.  $\|\Delta T^n\|_\infty$  for TEST1a.*

2. *TEST1b* (Figure 5.4) is a test case for the blood flow source term. The sagittal views in Figure 5.4 show off the distributing effect of the blood flow. Each temperature maximum is successively decreased and the heat energy is uniformly distributed over the whole body. The boundary layers with contact to the air are warmed for the time being ( $t \leq 12$  min.). However, the heat production and the distributing blood flow cannot maintain this state. The heat losses to the surrounding air are too large and cool down the boundary layers again. As a

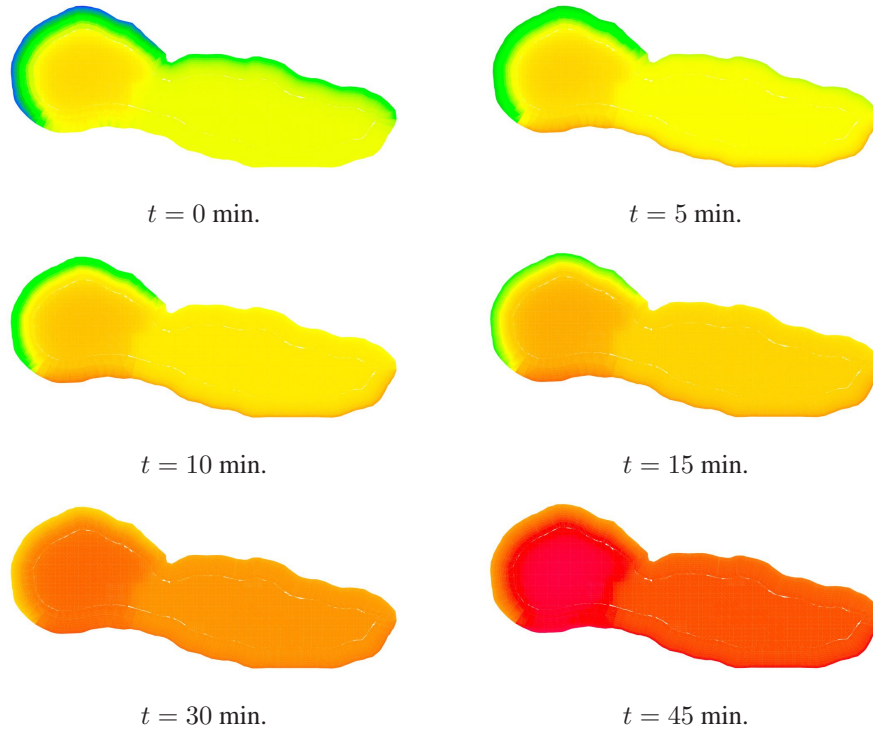


FIG. 5.6. TEST2.

result, steep temperature gradients can be observed in the steady state solution ( $t = 60$  min.; see also Figure 5.5).

3. In TEST2 (Figures 5.6 and 5.7) a heated mattress is used. As expected the boundary layers with contact to the air as well as those with contact to the mattress are warmed during the first ten minutes. Subsequently the whole body is uniformly warmed and a temperature maximum is built up in the brain, which extends through the back of the head to the heated mattress. The plots in Figure 5.7 show the surface temperature distributions of the steady state solution after  $t = 45$  min.. The simultaneous effects of the radiant warmer and the heated mattress are evident. The corresponding sagittal- and coronal intersections in Figure 5.7 show off the maximum in the head as well as the warming of the whole body including the periphery.

These results show that the model and the developed method nicely yield the expected temperature distributions. Especially the effects of the source terms and the boundary conditions are modeled correctly. Thus, the method is suitable for the solution of the bio-heat-transfer-equation and can be used to analyze the thermoregulatory phenomena of premature infants. The required computing time is moderate.

**6. Conclusions.** The development of a finite volume method for the simulation of temperature distributions in premature infants has been presented. The method is an improvement of previous ones since it can be applied to complex realistic geometries. The use of a semi-implicit BDF-method guarantees a stable and accurate time-integration. The arising large, sparse linear systems have been solved efficiently with the BiCGStab algorithm with ILU preconditioning. The numerical test runs show that realistic results which can be achieved

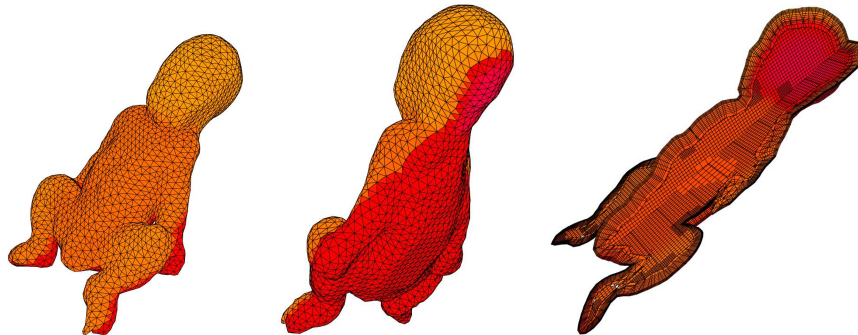


FIG. 5.7. TEST2 at  $t = 45$  min.

with moderate computation times. Thus, the developed method is a proper tool to analyze systematically the thermoregulation of premature infants.

#### REFERENCES

- [1] M. ALONSO AND E. J. FINN, *Physics*, Addison-Wesley Publishing Co., Amsterdam, 1992.
- [2] U. M. ASCHER, S. J. RUUTH, AND B. T. R. WETTON, *Implicit-explicit methods for time-dependent partial differential equations*, SIAM J. Numer. Anal., 32 (1995), pp. 797–823.
- [3] M. BREUSS, B. FISCHER, AND A. MEISTER, *The unsteady thermoregulation of premature infants - a model and its application*, in Proceedings of the GAMM-Workshop: Discrete Modelling and Discrete Algorithms in Continuum Mechanics, T. Sonar and I. Thomas, eds., Logos, Berlin, 2001, pp. 47-56.
- [4] O. BUSSMANN, *Modell der Thermoregulation des Früh- und Neugeborenen unter Einbeziehung der thermischen Reife*, Dissertation, Medizinische Universität zu Lübeck, Institut für Medizintechnik, Lübeck, 2000.
- [5] K. DEKKER AND J. G. VERWER, *Stability of Runge-Kutta Methods for Stiff Nonlinear Differential Equations*, North-Holland Publishing Co., Amsterdam, 1984.
- [6] F. A. DUCK, *Physical Properties of Tissue - 1. Mammals*, Academic Press, London, 1990.
- [7] A. FANAROFF AND R. MARTIN, *General principles of thermoregulation in the newborn*, in Neonatal-Perinatal Medicine, Diseases of the Fetus and Infant, A. Fanaroff and R. Martin, eds., Mosby, St. Louis, 1988, pp. 397-416.
- [8] D. FENNER, *Dreidimensionale Simulation der Thermoregulation von Früh- und Neugeborenen: Numerik und Visualisierung*, Diplomarbeit, Universität Hamburg, Fachbereich Mathematik, Hamburg, 2003.
- [9] J. H. FERZIGER AND M. PERIC, *Computational Methods for Fluid Dynamics*, Springer-Verlag, Berlin, 1999.
- [10] B. FISCHER, M. LUDWIG, AND A. MEISTER, *The thermoregulation of infants: Modeling and numerical simulation*, BIT, 41 (2001), pp. 950-966.
- [11] H. FRANKENBERGER AND A. GÜTHE, *Inkubatoren*, Verlag TÜV Rheinland, 1991.
- [12] E. HAIRER AND G. WANNER, *Solving Ordinary Differential Equations. II*, Springer-Verlag, Berlin, 1996.
- [13] J. KOCH, *Calculation Program Heat Balance, Version 2.0a*, Dräger Research, Lübeck, 1994.
- [14] ———, *Simulation Program Baby Thermoregulation*, Dräger Research, Lübeck, 2000.
- [15] W. LORENSEN AND E. HARVEY, *Marching cubes: A high resolution 3D surface construction algorithm*, in Computer Graphics (SIGGRAPH 87 Proceedings), M. C. Stone, ed., ACM, New York, 1987, pp. 163-170.
- [16] M. LUDWIG, *Ein Finite-Volumen-Verfahren zur numerischen Simulation der Temperaturverteilungen in Frühgeborenen*, Dissertation, Universität zu Lübeck, Institut für Mathematik, 2006.
- [17] H. H. PENNES, *Analysis of tissue and arterial blood temperatures in the resting human forearm*, J. Appl. Physiol., 1 (1998), pp. 5–34.
- [18] G. SIMBRUNER, *Thermodynamic Models for Diagnostic Purposes in the Newborn and Fetus*, Facultas Verlag, Wien, 1983.
- [19] H. A. VAN DER VORST, *Bi-CGSTAB: A fast and smoothly converging variant of Bi-CG for the solution of nonsymmetric linear systems*, SIAM J. Sci. Statist. Comput., 13 (1992), pp. 631–644.
- [20] M. WRONNA, *Ein Finite-Volumen-Verfahren zur dreidimensionalen und zeitgenauen Integration der Wärmeleitungsgleichung in Festkörpern aus unterschiedlichen Materialien*, Diplomarbeit, Universität zu Lübeck, Institut für Mathematik, 2004.